ELSEVIER

Journal of Quantitative Spectroscopy & Radiative Transfer 109 (2008) 974–994

Journal of Quantitative Spectroscopy & Radiative Transfer

www.elsevier.com/locate/jqsrt

Multispectrum analysis of the v_4 band of CH_3CN: Positions, intensities, self- and N_2-broadening, and pressure-induced shifts

C.P. Rinsland[a,*], V. Malathy Devi[b], D. Chris Benner[b], T.A. Blake[c], R.L. Sams[c], L.R. Brown[d], I. Kleiner[e], A. Dehayem-Kamadjeu[e], H.S.P. Müller[f], R.R. Gamache[g], D.L. Niles[g], T. Masiello[c]

[a]*NASA Langley Research Center, Mail Stop 401A, Hampton, VA 23681-2199, USA*
[b]*Department of Physics, The College of William and Mary, Box 8795, Williamsburg, VA 23187-8795, USA*
[c]*Pacific Northwest National Laboratory, P.O. Box 999, Mail Stop K8-88, Richland, WA 99352, USA*
[d]*Jet Propulsion Laboratory, California Institute of Technology, 4800 Oak Grove Drive, Pasadena, CA 91109, USA*
[e]*Laboratoire Interuniversitaire des Systèmes Atmosphériques, Universités Paris 7 et Paris 12 et CNRS, 61 av. General de Gaulle, 94010 Créteil, France*
[f]*I. Physikalisches Institut, Universität zu Köln, Zülpicher Str. 77, 50937 Köln, Germany*
[g]*Department of Environmental, Earth and Atmospheric Sciences, University of Massachusetts Lowell, Lowell, MA 01854, USA*

Received 17 October 2007; received in revised form 28 November 2007; accepted 30 November 2007

Abstract

A multispectrum nonlinear least-squares fitting technique was applied to measure accurate zero-pressure line center positions, Lorentz self- and nitrogen (N_2)-broadened half-width coefficients, and self- and N_2-pressure-induced shift coefficients for over 700 transitions in the parallel v_4 band of CH_3CN near 920 cm^{-1}. Fifteen high-resolution (0.0016 cm^{-1}) laboratory absorption spectra of pure and N_2-broadened CH_3CN recorded at room temperature using the Bruker IFS 125HR Fourier transform spectrometer located at the Pacific Northwest National Laboratory (PNNL) in Richland, Washington, USA, were analyzed simultaneously assuming standard Voigt line shapes. Short spectral intervals containing manifolds of transitions from the same value of J were fitted together. In all, high-precision line parameters were obtained for $P(44)$–$P(3)$ and $R(0)$–$R(46)$ manifolds. As part of the analysis, quantum assignments were extended, and the total internal partition function sum was calculated for four isotopologs: $^{12}CH_3^{12}CN$, $^{13}CH_3^{12}CN$, $^{12}CH_3^{13}CN$, and $^{13}CH_3^{13}CN$. Measurements of N_2 broadening, self-broadening, N_2-shift, and self-shift coefficients for transitions with J up to 48 and K up to 12 were measured for the first time in the mid-infrared. Self-broadened half-width coefficients were found to be very large (up to $\sim$2 cm^{-1} atm^{-1} at 296 K). Ratios of self-broadened half-width coefficients to N_2-broadened half-width coefficients show a compact distribution with rotational quantum number in both the P and R branches that range from $\sim$4.5 to 14 with maxima near $|m| = 24$, where $m = -J''$, J'', and $J'' + 1$ for P, Q, and R lines, respectively. Pressure-induced shifts for N_2 are small (few exceed $\pm$0.006 cm^{-1} atm^{-1} at 294 K) and are both positive and negative. In contrast, self-shift coefficients are large (maxima of about $\pm$0.08 cm^{-1} atm^{-1} at 294 K) and are both positive and negative as a function of

*Corresponding author. Tel.: +1 7578642699; fax: +1 7578648197.
E-mail addresses: curtis.p.rinsland@nasa.gov (C.P. Rinsland), Malathy.D.Venkataraman@nasa.gov (V. Malathy Devi), dcbenn@wm.edu (D. Chris Benner), ta.blake@pnl.gov (T.A. Blake), robert.sams@pnl.gov (R.L. Sams), Linda.R.Brown@jpl.nasa.gov (L.R. Brown), kleiner@lisa.univ-paris12.fr (I. Kleiner), dehayem@lisa.univ-paris12.fr (A. Dehayem-Kamadjeu), hspm@ph1.uni-koeln.de (H.S.P. Müller), Robert_Gamache@uml.edu (R.R. Gamache), dlniles@gmail.com (D.L. Niles), tony.masiello@nist.gov (T. Masiello).

0022-4073/$ - see front matter
doi:10.1016/j.jqsrt.2007.11.013

rotational quantum numbers. The present measured half-widths and pressure shifts in v_4 were compared with corresponding measurements of rotational transitions.

Keywords: CH_3CN; Atmosphere of Titan; Remote sounding; Fourier transform infrared (FTIR) spectroscopy; Pressure broadening; Pressure-induced shifts; Spectral line shape; Partition function; Transmission and scattering of radiation

1. Introduction

Methyl cyanide (acetonitrile, ethanenitrile, CH_3CN) is a molecule of atmospheric and astronomical importance. It has been measured by remote sensing in the Earth's atmosphere [1–3], in comets [4], and in interstellar molecular clouds [5]. It is also a constituent in the atmosphere of Titan, Saturn's largest moon [6,7], which has the densest nitrogen (N_2)-dominated atmosphere in the solar system. Photochemistry in the upper atmosphere of Titan leads to the production of hydrocarbons, and dissociation of N_2 leads to the production of nitriles. Methyl cyanide is the simplest organic nitrile with detection in the stratosphere reported from heterodyne ground-based microwave measurements [8,9].

Fourier transform spectrometer (FTS) measurements of Titan's complex and rich organic atmosphere containing hydrocarbons and nitriles are now being recorded at medium ($2.54\,cm^{-1}$) and high spectral resolution ($0.53\,cm^{-1}$) from 10 to 600 and 600 to $1400\,cm^{-1}$ by the Cassini/composite infrared spectrometer (CIRS) in nadir mode during flybys [6,7]. As CH_3CN has spectral bands in both regions, room-temperature laboratory spectra of pure and N_2-broadened CH_3CN samples have been recorded at a high resolution of $0.0016\,cm^{-1}$ (corresponds to the Bruker instrument resolution of $0.0029\,cm^{-1}$) using the Bruker IFS 125HR FTS located at the Pacific Northwest National Laboratory (PNNL) in Richland, Washington, USA. The $920\,cm^{-1}$ v_4 band occurs in an open region of weak emission in CIRS spectra, and hence it is potentially a band useful for quantifying CH_3CN atmospheric profiles or determining upper limits from those measurements. An initial analysis of a series of laboratory spectra of that band provides measured line positions, absolute intensities, and the first N_2- and self-broadened half-widths and pressure-induced line shift coefficients in the infrared. A multispectrum nonlinear least-squares analysis technique [10] has been applied in order to maximize the accuracy of the retrieved parameters. Previously absorption cross sections of methyl cyanide at temperatures of 273, 298, and 323 K were recorded at $0.112\,cm^{-1}$ resolution covering $600–6500\,cm^{-1}$ using a Fourier tranform spectrometer and a custom flowing sample delivery system [11].

2. Measurements

Laboratory spectra of pure and N_2-broadened CH_3CN samples were recorded at room temperature with a Bruker IFS 125 HR Fourier transform spectrometer. The acetonitrile sample was obtained from Sigma-Aldrich: anhydrous acetonitrile, 99.8% purity, with water content less than 0.005%. Approximately 10 ml of acetonitrile was transferred from the stock bottle to a cold finger containing dried calcium sulfate pellets (Drierite). The cold finger was attached to a metal vacuum manifold where the contents of the cold finger were degassed three times at liquid N_2 temperature. The acetonitrile was then transferred to a $50\,cm^3$ stainless steel cylinder with a welded bellows valve. The acetonitrile sample pressure was checked from time to time during the course of the experiment to make certain that no air had leaked into the sample cylinder. Ultra-high-purity N_2 (Oxarc) was used for the pressure-broadening studies. The N_2 was passed through a copper coil immersed in liquid N_2 to remove residual water and carbon dioxide before it was mixed with the acetonitrile. The carbonyl sulfide (OCS) used for calibration was from Matheson and was not further purified.

All spectra were recorded at room temperature using a "White-type" cell (Bruker model A134) to contain the gas samples. Wedged CsI windows were used with the White cell to reduce channeling in the spectra. The path lengths through the cell for the experiments described here are either 965 (1) or 2885 (1) cm. The room temperature was monitored with a platinum resistance thermometer placed near the White cell and was found to be typically 294.2 ± 0.5 K over the duration of one spectral measurement (10 h) and from day to day. The vacuum manifold was plumbed directly to the White cell, and the acetonitrile and N_2 were introduced from

the manifold to the White cell. The manifold was also used to evacuate the White cell. Three high-accuracy capacitance manometers (MKS instruments type 690A Baratrons) with 1, 10, and 1000 torr full-scale were connected to the vacuum manifold. The accuracy of the 1 and 10 torr manometers is $\pm 0.05\%$ of the pressure reading, while the accuracy of the 1000 torr manometer as stated by the manufacturer is $\pm 0.5\%$ of the pressure reading. Acetonitrile sample pressures were allowed to stabilize for approximately 30 min before the final pressure was recorded. The leak-up rate of the White cell when it is clean and well pumped is 2×10^{-5} torr min^{-1}.

A KBr beam splitter, Globar source, optical filter with 600–1000 cm^{-1} band pass, 5 kHz low-pass electronic filter, and HgCdTe detector were employed for these experiments. The optical path of the spectrometer was continuously evacuated to below 0.06 hPa for the duration of all spectral measurements. Spectra were recorded with an aperture diameter of 2 mm, 60 kHz scanner velocity, and instrument resolution of 0.0029 cm^{-1}. Bruker defines the maximum optical path difference (MOPD) as 0.9 resolution^{-1}, so in this case MOPD $= 0.9/0.0029$ cm$^{-1} = 310.345$ cm. For each background, sample, and calibration spectrum recorded, 512 single-sided interferograms were co-added. For FT conversion, a Mertz-phase correction, 1 cm^{-1} phase resolution, zero-filling factor of 1, and boxcar apodization were applied to the averaged interferograms. The nonlinearity correction for the HgCdTe detector was not used. For boxcar apodization, Bruker gives the instrument line width as $0.61/\text{MOPD} = 0.0020$ cm^{-1} FWHM. The signal-to-noise ratios for the recorded spectra are on the order of ~800:1.

Since it was not possible to keep two cells in tandem with the experimental setup used, the wavenumber calibration spectra were taken separately from the spectra of the target gas. The data collection procedure was as follows: first a background spectrum was recorded while the White cell was being continuously evacuated. Next a calibration spectrum was recorded using carbonyl sulfide. The White cell was then evacuated, flushed several times with dry N_2, and then evacuated until the base pressure of the cell was achieved ($<1 \times 10^{-5}$ torr). The acetonitrile spectra were then recorded starting with the lowest CH_3CN sample pressure and working to the highest sample pressure. The evacuation and flushing procedure described above was repeated between each sample spectrum. Then another background spectrum and calibration spectrum were recorded. All spectra with the White cell path length set at 965 cm were recorded first, followed by the spectra recorded with the 2885 cm path length.

Wedged CsI windows were used with the White cell to reduce channel spectrum. Even then some channel spectra arising from the optical system were observed in the data. These channel spectra were properly accounted for during the analysis using the multispectrum fittings. Using the background spectrum and the sample spectrum, the transmission spectrum was obtained for each scan. During the initial analysis, we tried using both the sample spectrum as well as the transmission spectrum. In the final analysis, except for one low-pressure pure CH_3CN spectrum all other spectra were transmission spectra.

As an example, a normalized transmission spectrum of pure CH_3CN covering the entire band is illustrated in Fig. 1. Strong apodization was applied in the process of converting the measured interferograms to spectra for display and then analysis. The band exhibits a prominent Q branch at 920 cm^{-1} in addition to well-defined P and R branch structures with maxima near 909 (P branch) and 933 cm^{-1} (R branch). A short spectral region (930–932 cm^{-1}) of the same spectrum with transitions from the ν_4 fundamental identified is shown in Fig. 2. The strongest line in each manifold is for $K = 3$. As indicated, lines of the $\nu_4 + \nu_8 - \nu_8$ hot band also produce prominent absorption features in this region, as well as in other regions of the spectra.

In Table 1 is shown a summary of the experimental conditions for the 15 spectra used in the analysis. All spectra were obtained at the same resolution of 0.0016 cm^{-1} (1/2 L, where L = MOPD). A total of nine spectra were recorded with pure CH_3CN, and those were used for measurement of intensities, self-broadened half-width, and self-shift coefficients. All were obtained with a cell path length of 965 cm. Six spectra recorded with mixtures of N_2 and CH_3CN at pressures of 30.28–80.09 torr were used for the analysis of N_2-broadened half-width and N_2-pressure-induced shift coefficients. All of those spectra were recorded with a cell path length of 2885 cm. The measurement temperatures of all but one spectrum were near 294 K.

The first step in using the multispectrum fitting technique is to perform the wavenumber calibration of all the data to be fit simultaneously. For the spectral band pass used in this analysis, the OCS line positions of the ν_2 band available from the National Institute of Standards and Technology (NIST) reference data produced by Maki and Wells were assumed [12]. The calibration correction factors in several spectra obtained within the

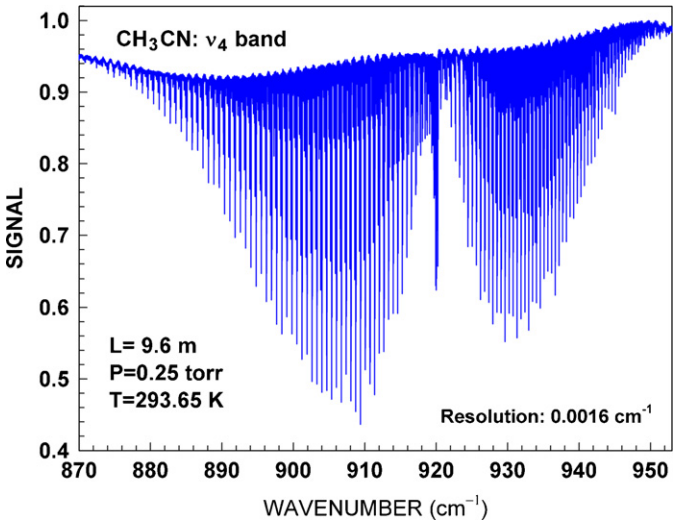

Fig. 1. Sample normalized spectrum of pure CH_3CN showing the entire v_4 band (870–953 cm^{-1} region). Pressure, temperature, and absorption path length are indicated.

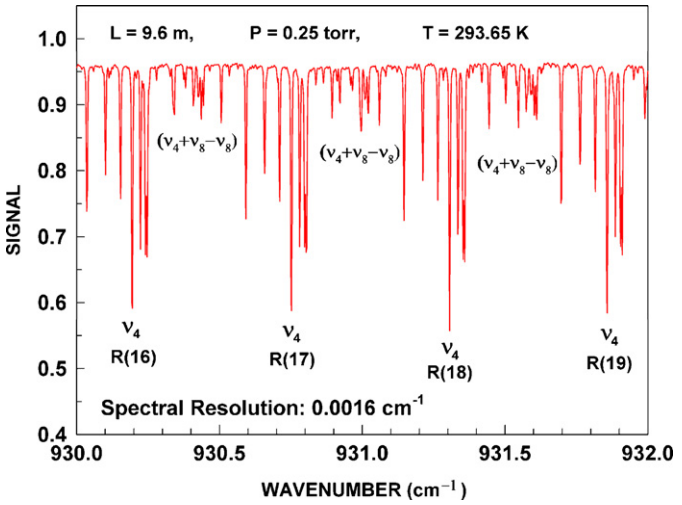

Fig. 2. Expanded plot of a short region of the spectrum of Fig. 1. The $R(16)$–$R(19)$ sequences of the v_4 band are identified. The locations of stronger features of the $v_4+v_8-v_8$ hot band are indicated.

period of a week were found to be within their mutual statistical uncertainties, $1.5\times10^{-6}\,cm^{-1}$. The precisions and absolute accuracies of the CH_3CN positions are somewhat worse, however, due to the complexity of the spectrum.

As discussed later in Section 3, limitations of the line parameters in developing a line list for the databases due to the effects of various resonances described above are a major consideration in the intensity analysis of the CH_3CN spectra. To evaluate the possible need for incorporating line mixing or speed dependence [13] into the model for the analysis of the spectra [10], we first fit the full set of PNNL spectra for sample spectral intervals assuming a Voigt line shape [14] based on a line list derived from line positions obtained by peak finding. An example of a multispectrum fit in the $P(9,K)$ manifold is shown in Fig. 3. As illustrated in this figure, the standard Voigt model [14] proved sufficiently accurate to fit the measurement set to the noise level without Dicke narrowing, line mixing, and/or speed dependence. Tick marks shown at the top of panel (b) correspond to the positions of lines included in the multispectrum fitting. Similarly, we show in Fig. 4 a

Table 1
Summary of the experimental conditions of the spectra

Temperature (K)	Broadening gas	Volume-mixing ratio	Optical path length (cm)[a]	Total sample pressure (torr)
293.7	CH_3CN	1.00	965	0.110
293.7	CH_3CN	1.00	965	0.250
293.7	CH_3CN	1.00	965	0.500
293.7	CH_3CN	1.00	965	0.382
293.7	CH_3CN	1.00	965	0.588
293.7	CH_3CN	1.00	965	0.804
293.7	CH_3CN	1.00	965	1.043
293.7	CH_3CN	1.00	965	1.521
293.7	CH_3CN	1.00	965	2.127
294.3	N_2	0.0457	2885	30.28
296.0[b]	N_2	0.0383	2885	30.87
293.7	N_2	0.0145	2885	41.78
294.3	N_2	0.0266	2885	63.75
293.7	N_2	0.0164	2885	70.17
294.3	N_2	0.0503	2885	80.09

760 Torr = 1 atm = 1013.25 hPa.
See text for uncertainties associated with sample temperature and pressure measurements.
[a]The uncertainty in path length is ±1 cm.
[b]The sample temperature for this spectrum was slightly higher than other data.

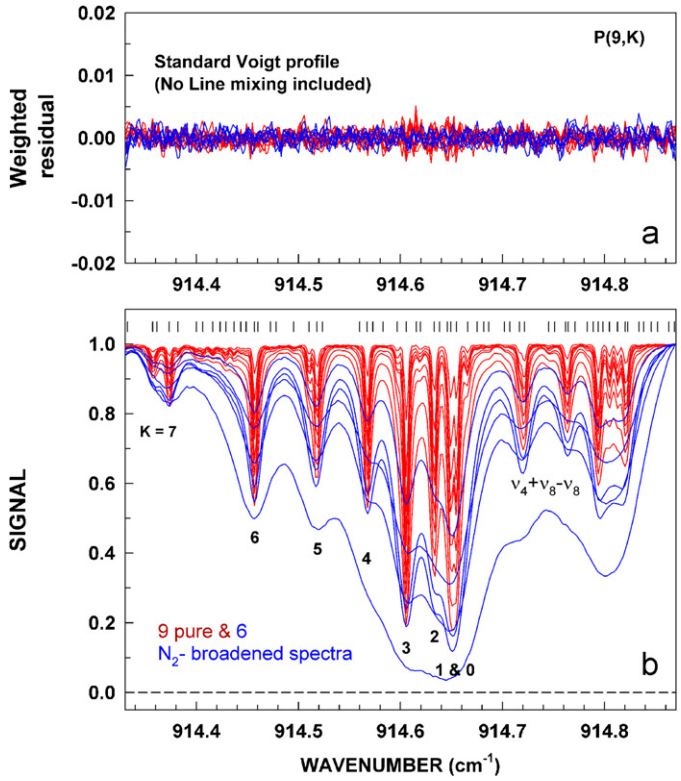

Fig. 3. $P(9, K)$ manifold fit obtained from nine pure and six N_2-broadened spectra assuming a standard Voigt line shape. All 15 observed spectra are shown in the lower panel with locations of the lines included in the multispectrum analysis shown by vertical tick marks in the lower panel. The 100% absorption line is shown by the dotted line at the bottom panel. The upper panel shows the fit residuals on an expanded vertical scale.

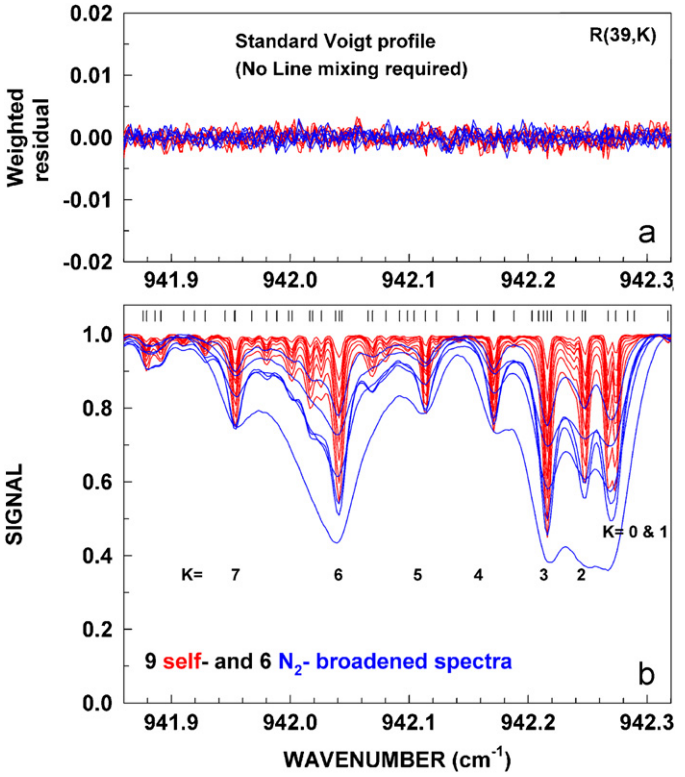

Fig. 4. $R(39, K)$ manifold fit obtained from a simultaneous fit to the full set of 15 spectra assuming a standard Voigt line shape. The tick marks shown at the top of the lower panel correspond to positions of lines included in the fit. The lower panel shows the 15 observed spectra with the assignments of strong features of ν_4 indicated. The upper plot illustrates the fit residuals on an expanded vertical scale.

multispectrum fit for the $R(39,K)$ manifold that includes nine pure CH_3CN and six N_2-broadened spectra. Analysis of the spectra near band center was limited by the complexity of the spectra and the high density of the lines. A Voigt line shape was also assumed in the analysis of millimeter heterodyne measurements of CH_3CN in Titan's upper atmosphere with satisfactory fits reported [9].

In the end, the zero-pressure line center positions (ν_0) in cm^{-1}, intensities in cm molecule^{-1} at 296 K, self- and N_2-broadened half-width coefficients, b_L^0(self) and $b_L^0(N_2)$ in $cm^{-1}\,atm^{-1}$ at 296 K, and self- and N_2-induced pressure-shift coefficients δ^0(self) and $\delta^0(N_2)$ in $cm^{-1}\,atm^{-1}$ at the sample temperature (Table 1) were determined for over 700 lines in the P and R branch manifolds of ν_4. The list of retrieved parameters with tentative quantum assignments is on deposit with the journal as a supplementary file (see Supplementary List). A sampling of these measurements is shown in Table 2 for features that appear near the $R(39,K)$ manifold. The other transitions include the high K transitions from $R(40,K)$ and hot bands like $\nu_4+\nu_8-\nu_8$. The measurements of blended lines tend to have greater uncertainties (e.g. $R(39,7)$). The values of half-width coefficients that were not adjusted in the least-squares fit were fixed to default values (in $cm^{-1}\,atm^{-1}$ at 296 K) of 0.13 (N_2 widths) and 1.5 (self-widths). In some instances where these values did not quite fit as judged from the fit residuals, their values were adjusted by trial and error until a good fit was obtained. The values for the pressure-shift coefficients that were not determined were fixed to zero during the least-squares analysis.

3. Analysis and results

A preliminary analysis of positions provided tentative quantum assignments for many P and R branch transitions of ν_4. The $\nu_4+\nu_8-\nu_8$ hot band, which could not be modeled satisfactorily beyond $K=5$, overlapped the Q branch of ν_4 so extensively that these measurements are not being reported at this time. In addition, the sample temperatures spanned over 2 K, requiring better knowledge of the total partition function

Table 2
A sample set of measurements in the $R(39,K)$ region of CH_3CN

ν (cm^{-1})	Int[a]	% u	$b_L^0(N_2)$[b]	% u	b_L^0(sf)[b]	% u	$\delta^0(N_2)$[c]	δ^0(sf)[c]	J'	K'	J''	K''
941.87927(2)	14.53	1.0	0.1250	1.0	0.905	2.1			40	8	39	8
941.88622(20)	3.16	5.4										
941.89133(3)	14.23	1.4	0.1365	1.0	1.406	2.1						
941.91050(15)	6.47	1.5										
941.92850(3)	11.65	1.5	0.1219	1.5	1.465	2.3						
941.94442(2)	1.90	6.3										
941.95314(7)	39.69	7.3	0.1200	1.9	0.813	10.2	−0.0021(15)	+0.002(32)	40	7	39	7
941.95467(15)	13.64	20.4										
941.96752(7)	7.61	2.7	0.1280	3.5	2.007	3.9						
941.98003(3)	13.76	1.4	0.1219	1.4	1.406	2.2						
941.98871(11)	4.12	2.9										
941.99849(19)	6.24	10.5										
942.00151(6)	19.59	3.6	0.1353	1.3	1.543	1.7						
942.01644(1)	32.61	0.6	0.1320	0.7	1.478	1.0						
942.02611(2)	25.12	0.8	0.1430	1.1	1.507	1.3						
942.03801(4)	38.06	2.3	0.1484	1.9	1.498	1.4						
942.04125(6)	56.67	3.2	0.1172	0.9	0.910	1.7	−0.0055(8)	−0.008(15)	40	6	39	6
942.04352(13)	21.82	9.6										
942.06537(24)	3.41	10.5										
942.06910(4)	20.00	2.1	0.1299	1.0	1.463	1.7						
942.08043(4)	12.12	1.6	0.1345	1.7	1.632	2.4						
942.09191(16)	2.95	4.4										
942.09858(7)	6.57	3.5	0.1365	3.2	1.363	5.0						
942.10414(25)	2.94	5.1										
942.11366(2)	35.99	0.4	0.1247	0.4	0.874	0.9	+0.0013(7)	−0.017(9)	40	5	39	5
942.12298(5)	5.13	2.9	0.1315	3.6	0.847	5.7						
942.14104(13)	2.97	3.7										
942.15700(20)	1.75	5.7										
942.17118(1)	45.55	0.3	0.1222	0.4	0.916	0.7	+0.0002(4)	−0.031(8)	40	4	39	4
942.18803(9)	4.71	3.8	0.1332	4.5	1.551	6.0						
942.21285(16)	11.98	7.7										
942.21603(2)	112.14	0.7	0.1227	0.3	0.915	0.7	+0.0013(3)	−0.037(8)	40	3	39	3
942.21945(26)	7.18	10.8										
942.23275(6)	12.19	2.4	0.1394	3.3	1.924	2.9						
942.23834(4)	16.86	1.8	0.1335	2.5	1.537	2.5						
942.24552(9)	18.49	7.0	0.1591	5.3	0.944	4.5			41	9	40	9
942.24805(3)	60.94	2.1	0.1159	1.2	0.926	0.9	−0.0059(9)	−0.037(12)	40	2	39	2
942.26721(10)	67.57	0.3	0.1255	0.6	0.908	0.6	−0.0029(7)	−0.039(7)	40	1	39	1
942.27361(10)	67.67	0.3	0.1224	0.5	0.893	0.6	−0.0016(7)	−0.020(6)	40	0	39	0
942.28350(15)	2.18	5.5										
942.28930(20)	1.73	6.3										
942.31736(15)	2.94	4.7			0.678	11.2						

Notes: % u values are the uncertainties of the adjacent coefficients in percent.
Assigned lines belong to the v_4 band. The majority of the unassigned lines are higher J or K v_4 lines or from hot bands such as $v_4+v_8-v_8$.
[a]Intensities are in 10^{-24} cm mol^{-1} at 296 K.
[b]The N_2 and self- (sf) half-width coefficients (b_L^0) are in cm^{-1} atm^{-1} at 296 K.
[c]Pressure-shift coefficients (δ^0) are in cm^{-1} atm^{-1} at 294 K (temperature of the sample).

and the lower state transition energies in order to adjust the line intensities properly while retrieving the positions and broadening coefficients.

3.1. Total internal partition function

As mentioned in Ref. [3], the HITRAN 2004 [15] and GEISA 2003 [16] databases do not include a calculation for the total internal partition sum (TIPS) for CH_3CN. The total internal partition function plays a

critical role in determining the temperature dependence of line intensities, and an incorrect partition function may lead to a systematic error in vertical profile retrievals from line-by-line data [17]. In this study, the total internal partition sum was calculated for four isotopologs: $^{12}CH_3^{12}CN$, $^{13}CH_3^{12}CN$, $^{12}CH_3^{13}CN$, and $^{13}CH_3^{13}CN$. The calculations employed the product approximation for the TIPS:

$$Q(T) = Q_{vib}(T)Q_{rot}(T), \tag{1}$$

where Q_{vib} and Q_{rot} are the vibrational and rotational partition sums. The calculation of Q_{vib} was made using the harmonic approximation [18]

$$Q_{vib}(T) = \prod \frac{1}{1 - e^{v_i/kT}}, \tag{2}$$

where v_i are the fundamental vibrational frequencies of CH_3CN and k is the Boltzmann constant. The values of the fundamental vibrational frequencies for the different isotopologs listed in Table 3 are from Duncan et al. [19] unless otherwise noted where the Duncan et al. values [19] were replaced by more accurate values [20–22]. For the $^{13}CH_3^{13}CN$ isotopolog the fundamental vibrational frequencies were estimated from the values from the other isotopologs.

The rotational partition sums were calculated using McDowell's [23] analytical formula for symmetric tops. The rotational constants for $^{12}CH_3^{12}CN$ were taken from Simeckova et al. [24], those for $^{13}CH_3^{12}CN$ and $^{12}CH_3^{13}CN$ were from Boucher et al. [25], and those for $^{13}CH_3^{13}CN$ were estimated from the values from the other isotopologs. These constants are presented in Table 4. The spin statistics for CH_3CN are for K divisible by 3 including zero $g_s = 4$ and K not divisible by 3 $g_s = 2$. Lamda doubling gives the symmetry factor in McDowell's [23] formula

$$\bar{g}_s = \prod \frac{2(I_H + 1)^3}{3} = \frac{8}{3}.$$

Hyperfine structure was not considered; thus, the state independent degeneracy factors ($\Pi(2I_i + 1)$ are 3, 6, 6, and 12 for $^{12}CH_3^{12}CN$, $^{13}CH_3^{12}CN$, $^{12}CH_3^{13}CN$, and $^{13}CH_3^{13}CN$, respectively.

Calculations of Q_{vib} and Q_{rot} were made for each isotopolog at temperatures ranging from 60 to 3010 K in 1 K steps. The total internal partition sums were determined from Q_{vib} and Q_{rot}. The TIPS data were then taken at 25 K intervals and a code was written to recalculate the TIPS using a 4-point Lagrange interpolation scheme, thus providing rapid and accurate recall of the TIPS in the temperature range 70–3000 K. This code is available from one of the authors (R.R.G.). Table 5 gives the TIPS for the isotopologs considered at a number of temperatures in the range 150–350 K.

We can obtain an estimate of our value by comparing with the classical value using the formula given by Herzberg [18]. Removing the symmetry factor from our value ($3 \times 8/3$) gives the value of 7588, which can be compared with the classical value of 7574.6. Thus, we have excellent agreement with the classical value.

Table 3
Fundamental vibrational frequencies (in cm^{-1}) for the isotopologs of CH_3CN used in the calculation of the vibrational partition sums

Fundamental	Degeneracy	$^{12}CH_3^{12}CN$	$^{13}CH_3^{12}CN$	$^{12}CH_3^{13}CN$	$^{13}CH_3^{13}CN$[a]
v_1	1	2953.92	2949.63	2953.65	2949.6
v_2	1	2266.45	2259.55	2216.13	2215.0
v_3	1	1385.171[b]	1380.0	1390.0	1380.0
v_4	1	920.290284[c]	903.22	915.72	900.0
v_5	2	3009.16	2999.1	3009.05	2999.0
v_6	2	1448.03	1446.95	1448.03	1447.0
v_7	2	1041.854706[c]	1032.49	1036.37	1030.0
v_8	2	365.015965[d]	364.25	356.88	357.0

[a]Estimated from Refs. [20–22].
[b]Ref. [20].
[c]Ref. [21].
[d]Ref. [22].

Table 4
Constants (in cm^{-1}) used in the calculation of the rotational partition sums

Constant	$^{12}CH_3^{12}CN$[a]	$^{13}CH_3^{12}CN$[b]	$^{12}CH_3^{13}CN$[b]	$^{13}CH_3^{13}CN$[c]
A	5.27361573	5.247	5.247	5.247
B	0.306842247	0.29798328	0.30669047	0.297
D_J	$1.27003028 \times 10^{-7}$	1.2268×10^{-7}	1.273×10^{-7}	1.23×10^{-7}
D_{JK}	$5.91758716 \times 10^{-6}$	5.59220×10^{-6}	5.87560×10^{-6}	5.558×10^{-6}
D_K	9.43986×10^{-5}	9.507×10^{-5}	9.473×10^{-5}	9.505×10^{-5}
H_J	-8.806×10^{-15}	0.0	0.0	0.0
H_{JK}	3.41036×10^{-11}	0.0	0.0	0.0
H_{KJ}	2.02103×10^{-10}	0.0	0.0	0.0
H_K	4.403×10^{-9}	0.0	0.0	0.0
Sym factor	$3.0 \times 8/3$	$6.0 \times 8/3$	$6.0 \times 8/3$	$12.0 \times 8/3$

[a]From Ref. [20].
[b]From Ref. [21].
[c]Estimated from Refs. [24,25].

Table 5
CH_3CN partition function values at different temperatures

T (K)	$^{12}CH_3^{12}C^{14}N$		$^{12}CH_3^{13}C^{14}N$	
	Q_{rot}	Q_{vib}	Q_{rot}	Q_{vib}
150	2.1458×10^4	1.0635	4.3046×10^4	1.0688
175	2.7040×10^4	1.1085	5.4244×10^4	1.1166
200	3.3037×10^4	1.1652	6.6275×10^4	1.1763
225	3.9423×10^4	1.2332	7.9086×10^4	1.2477
250	4.6176×10^4	1.3126	9.2632×10^4	1.3301
275	5.3276×10^4	1.4039	1.0688×10^5	1.4260
296	5.9498×10^4	1.4903	1.1936×10^5	1.5161
300	6.0709×10^4	1.5079	1.2179×10^5	1.5343
325	6.8460×10^4	1.6256	1.3734×10^5	1.6569
350	7.6516×10^4	1.7583	1.5350×10^5	1.7951
	$^{13}CH_3^{12}C^{14}N$		$^{13}CH_3^{13}C^{14}N$	
	Q_{rot}	Q_{vib}	Q_{rot}	Q_{vib}
150	4.4303×10^4	1.0640	8.8899×10^4	1.0688
175	5.5828×10^4	1.1094	1.1203×10^5	1.1166
200	6.8210×10^4	1.1665	1.3687×10^5	1.1764
225	8.1396×10^4	1.2351	1.6333×10^5	1.2480
250	9.5338×10^5	1.3153	1.9131×10^5	1.3314
275	1.1000×10^5	1.4076	2.2073×10^5	1.4272
296	1.2285×10^5	1.4950	2.4650×10^5	1.5179
300	1.2535×10^5	1.5128	2.5152×10^5	1.5362
325	1.4135×10^5	1.6320	2.8363×10^5	1.6597
350	1.5798×10^5	1.7666	3.1701×10^5	1.7990

We also compared our rotational partition sum to that listed in the Jet Propulsion Laboratory (JPL) catalog [26] for $^{12}CH_3^{12}CN$. At 300 K Q_{rot} (JPL) = 41,079.2740 and Q_{rot} (this work) = 60,709.144. In fact, the JPL value is based just on the levels of the ground state and the lowest fundamental. Retrievals of CH_3CN atmospheric profiles from balloon-borne tropospheric and stratospheric solar spectra [3] assumed a partition function calculation based on the locations and degeneracies of the fundamental bands of $^{12}CH_3^{12}CN$ following a procedure used for analysis of solar spectra recorded by the Atmospheric Trace MOlecule Spectroscopy experiment [27].

3.2. Positions, assignments, and lower state energies

There are numerous interactions between $v_4 = 1$ and adjacent states. Starting at low K, these are $K = 5$ with $K = 8$ of $v_8 = 2^0$ (very weak); $K = 5$ and 6 with $K = 6$ and 7 of $v_8 = 2^{-2}$ (weak with larger local effects); $K = 6$ and 7 with $K = 4$ and 5 of $v_7 = 1^{+1}$ (weak with larger local effects); and $K = 7$ with $K = 5$ of $v_8 = 3^{+1}$ (weak with larger local effects); rather pronounced perturbations of the positions occur because of a Fermi-type interaction with $v_8 = 3^{+3}$ especially around $K = 7$ and 8. At even higher K, further interactions may play a role, but their effect on the intensities likely will be very local, with the possible exception of the weak Coriolis interaction between $v_4 = 1$ and $v_7 = 1$. Most of these interactions have been outlined already by Tolonen et al. [21]. Past studies were used to generate an initial prediction of energy levels based on measurements and assignments from the $v = 0$ (pure rotation) region [28–30], the v_8 band region by Müller et al. [31] and Bocquet et al. [32], $2v_8$, and v_4, v_7, and $3v_8$ bands by Tolonen et al. [21] combined with new extended assignments for the fundamentals. We note the resonances similar to those for CH_3CN have also been studied and modeled in the both the v_8 and $2v_8$ bands of CD_3CN [33].

Initially, line positions of the v_4 band were fit based on the work of Tolonen et al. [21] and Koivusaari et al. [22] using the C_{3v} point group analysis program of Tarrago et al. [34]. New assignments were extended to higher J and K transitions. Further improvements will require a global fit of line positions and intensities of v_4 transitions with those from the v_7 and $2v_8$ bands. The process of assigning high J and K transitions is a work in progress. The present study of positions and intensities of the v_4 CH_3CN lines is the most comprehensive study thus far and involves transitions from other (v_7 and $2v_8$) bands. As a result, a separate publication resulting from such a study is well under way and will be reported. This section is intended to give the reader an overview of that separate effort to deal with the analysis of a difficult polyad. The widths, shifts, and other coefficients of the transitions that have been measured and reported in this study (Sections 3.3 and 3.4) are unaffected by such interactions.

3.3. N_2- and self-broadened Lorentz half-width coefficients

The pressure-broadening and pressure-shift coefficients were determined using the following expressions [35]:

$$b_L(p,T) = p\left[b_L^0(N_2)(p_0,T_0)(1-\chi)\left[\frac{T_0}{T}\right]^{n1} + b_L^0(\text{self})(p_0,T_0)\chi\left[\frac{T_0}{T}\right]^{n2}\right], \tag{3}$$

$$v = v_0 + p[\delta^0(N_2)(1-\chi) + \delta^0(\text{self})\chi], \tag{4}$$

$$\delta^0(T) = \delta^0(T_0) + \delta'(T - T_0). \tag{5}$$

In the above equations, for $T_0 = 296\,\text{K}$ and $p_0 = 1\,\text{atm}$, b_L^0 and δ^0 represent pressure-broadening and pressure-shift coefficients (in $\text{cm}^{-1}\,\text{atm}^{-1}$ at 296 K), respectively. b_L (p, T) is the Lorentz half-width (in cm^{-1}) of the spectral line at pressure p and temperature T, $b_L^0(\text{gas})(p_0, T_0)$ is the Lorentz half-width coefficient of the line at the reference pressure p_0 and temperature T_0 of the broadening gas (either N_2 or CH_3CN), and χ is the ratio of the partial pressure of CH_3CN to the total sample pressure in the cell. In the analysis, for the temperature dependences of N_2- and self-broadened half-width coefficients, we assumed values of n_1 and n_2 to be equal to 0.75, a value usually assumed as the temperature-dependence exponent for gases such as CO_2 and CH_4.

In Fig. 5, the N_2- and the self-broadened half-width coefficients are plotted vs. m for the v_4 P and R branches, where m is $-J''$ for P-branch lines and $J''+1$ for R-branch lines. Vertical lines indicate the one standard deviation statistical uncertainty of the measurements. We note that outlying points may be caused by an incorrect quantum assignment. Self-broadened half-width coefficients show a wide range of values with a different pattern for distribution. Self-broadened half-width coefficients as high as $\sim 2.0\,\text{cm}^{-1}\,\text{atm}^{-1}$ were measured for transitions with $|m|$ near 24 (Fig. 5(b)). The self-broadened half-width coefficients for low values of m (0–6) in the R branch initially decrease from $\sim 1.8\,\text{cm}^{-1}\,\text{atm}^{-1}$ at 296 K to about $1.0\,\text{cm}^{-1}\,\text{atm}^{-1}$ at 296 K,

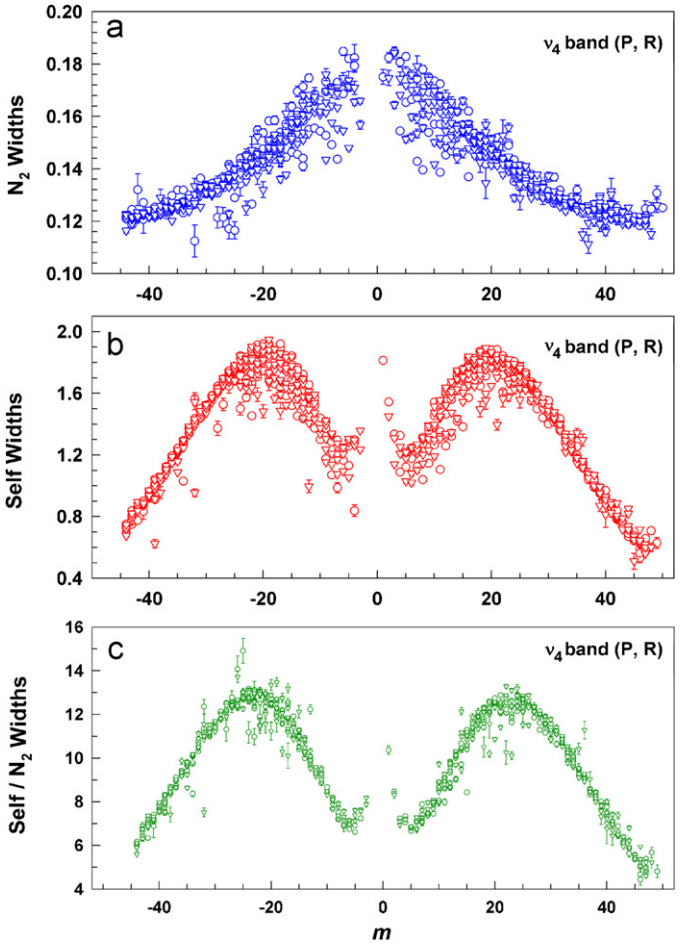

Fig. 5. Measured N_2- and self-broadened half-width coefficients (in $cm^{-1}\,atm^{-1}$ at 296 K) plotted as a function of m are shown in panels (a) and (b), respectively. Self-broadened half-width coefficients are almost an order of magnitude larger than the corresponding N_2-broadened half-width coefficients. The ratios of self- to N_2-broadening coefficients vs. m are plotted in (c). Where no error bars are visible the uncertainties are smaller than the size of the symbol used.

then increase to a maximum value of $\sim$1.9 $cm^{-1}\,atm^{-1}$ at 296 K near $m = 24$, and then slowly fall off to $\sim$0.5 $cm^{-1}\,atm^{-1}$ at 296 K with $m = 46$. In the P branch we see a similar pattern except that for low values of m a smaller decrease is observed than in the R branch. In Fig. 5(c), the ratios of self- to N_2-broadened half-width coefficients are plotted vs. m. These ratios vary from $\sim$4.5 at high m ($m = \sim$46) to $\sim$14 near $m = 24$.

The variation with K is shown in Fig. 6(a and b) where the N_2-broadened half-width coefficients and self-broadened half-width coefficients in the P and R manifolds are plotted vs. $K + 0.010$ ($|m| - K$), and $|m| = J''$ for P-branch transitions and $|m| = J'' + 1$ for R-branch transitions. The term 0.010 ($|m| - K$) offsets the plotting symbols to reveal the trend in broadening coefficients with $|m|$ for each value of K. N_2-broadened half-width coefficients show decreasing widths for increasing K and $|m|$. The characteristic pattern observed for self-broadened half-width coefficients vs. $|m|$ seen in Fig. 5(b) is clearly seen in Fig. 6(b). The values of half-width coefficients for $K + 0.010$ ($|m| - K$) < 11 are shown in Fig. 6(a and b); values obtained for higher K are not reported at this time.

The N_2- and self-broadened half-width coefficients plotted vs. $|m|$ are displayed in Fig. 7 for selected values of K. The patterns of the distributions are compact and significantly different. Half-width coefficients for N_2 broadening for all K peak at low $|m|$ with progressively lower maximum widths at higher K. Peaks of self-broadened half-width coefficients show a more complex distribution with $|m|$. For both N_2- and

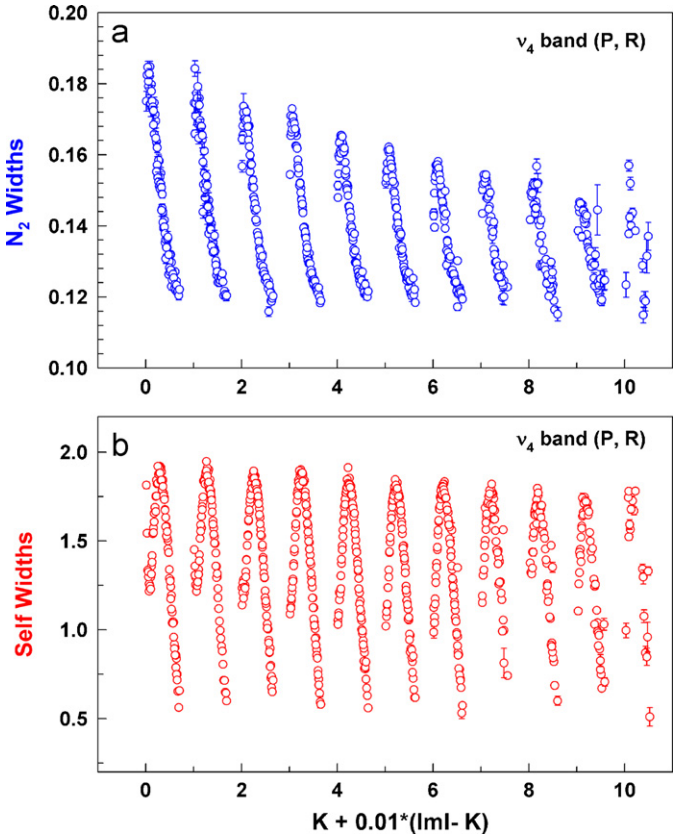

Fig. 6. N_2 half-width (upper panel) and self-half-width coefficients (upper panel) ($cm^{-1}\,atm^{-1}$ at 296 K) in the P and R manifolds of the ν_4 band plotted vs. $K+0.010$ ($|m|-K$), where $|m| = J''$ for P-branch transitions and $|m| = J''+1$ for R-branch transitions. The quantity 0.010 ($|m|-K$) is used to offset the symbols for trend recognition. Where no error bars are visible, the uncertainties are smaller than the size of the symbol used.

self-broadened half-width coefficients the values for a pair of lines with the same $|m|$ and K from the P and R branches are close to the same value (open vs. filled symbols).

3.4. N_2- and self-pressure-induced shift coefficients

As seen in Fig. 8(a and b), the observed N_2- and self-pressure-induced shift coefficients are both negative and positive. The N_2 shift coefficients are small and vary from ~0.012 to $+0.012\,cm^{-1}\,atm^{-1}$ at ~294 K; few exceed $\pm 0.006\,cm^{-1}\,atm^{-1}$ at 294 K, with no obvious dependence in the pressure-shift coefficient with m. In contrast, self-shift coefficients are large, ranging from ~−0.08 to $+0.10\,cm^{-1}\,atm^{-1}$ at ~294 K (maxima of about $\pm 0.08\,cm^{-1}\,atm^{-1}$) with compact and well-defined distributions as a function of m.

The patterns are further investigated in Fig. 9 by showing the measured N_2 and self-shift coefficients vs. $|m|$ for specific values of K (e.g., $K = 0,1,3,6$). Again, the patterns for N_2-shift coefficients (left column) are quite different from those for self-shift coefficients (right column). Apart from the magnitude of the two types (N_2 and self) of shift coefficients, N_2-shift coefficients are similar (open vs. filled symbols) for P- and R-type transitions (left panels), but self-shift coefficients are anti-correlated (right panels). In other words, the self-shift coefficients in P and R lines vary opposite with $|m|$, but cross each other around $|m| = \sim 22$. Another view of this behavior is seen in Fig. 10 where N_2- and self-shift coefficients are plotted vs. K for select $|m|$ for P- and R-branch transitions to emphasize the variation of the two broadening gases by quantum numbers. There are some small differences in the N_2-shift coefficients for P and R lines in a given $|m|$ (e.g., $|m| = 5$]); for self-broadening, the shift coefficients are nearly equal in magnitude but have opposite signs for pairs of P and R lines of the same $|m|$ and K. The horizontal dashed line in each panel represents a shift coefficient of zero.

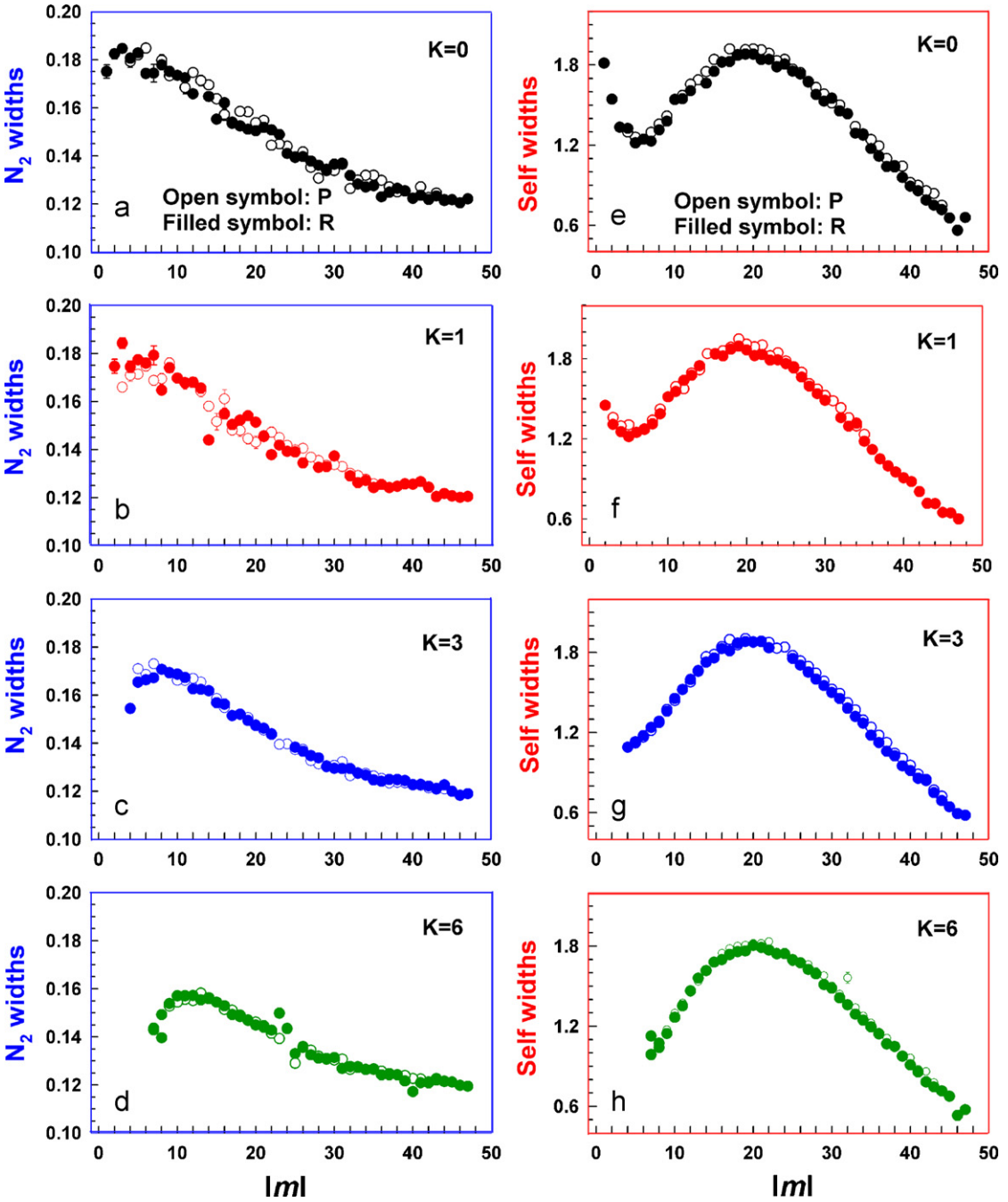

Fig. 7. N_2- and self-broadened half-width coefficients ($cm^{-1}\,atm^{-1}$ at 296 K) plotted vs. $|m|$ for select values of K. Open symbols correspond to P-branch transitions and filled symbols correspond to R-branch transitions to show that P and R branch widths are similar for transitions of the same $|m|$ and K. In most cases, the uncertainties in the measured broadening coefficients are smaller than the size of the symbol used and are not visible in the plots. For brevity, broadening coefficients are written as widths in labeling the y-axes.

In Fig. 11 are displayed Lorentz half-width coefficients vs. pressure-shift coefficients for N_2 (Fig. 11a) and self-broadening (Fig. 11b) in order to investigate any correlations between the shifts and widths coefficients. In both cases, we see that the shift coefficients become more positive with increasing broadening coefficients.

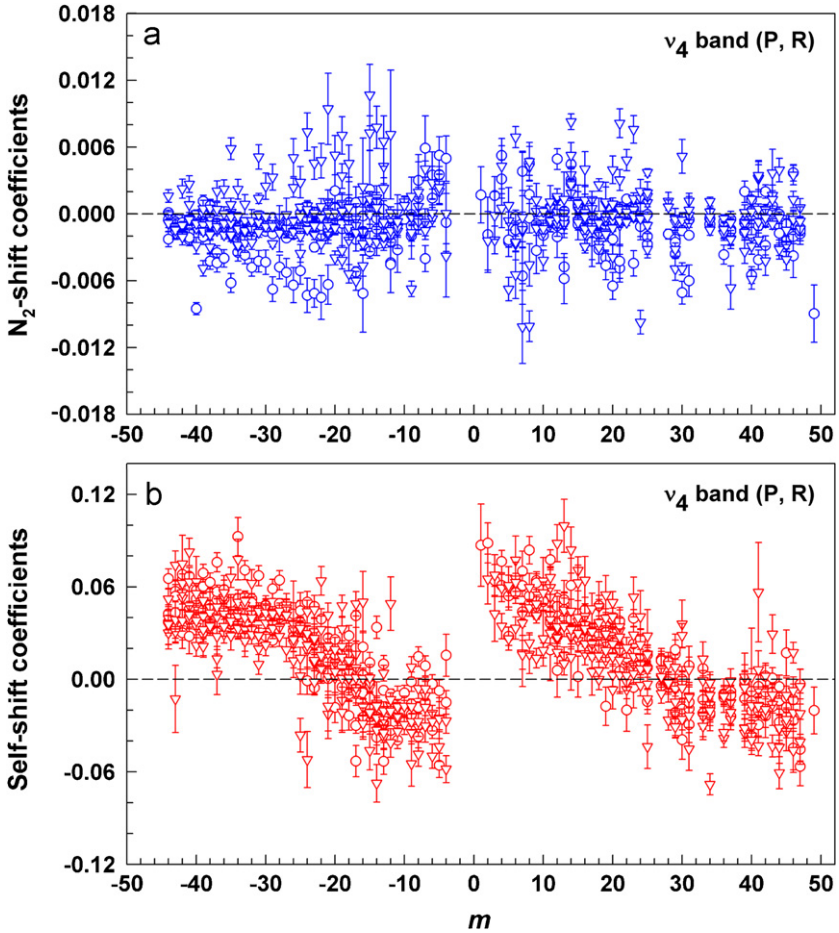

Fig. 8. N_2-shift (upper panel) and self-shift (lower panel) coefficients in $cm^{-1}\,atm^{-1}$ at ~294 K vs. m for the P and R branch lines in the ν_4 band. Dashed horizontal line indicates a shift coefficient of zero.

The absolute accuracy in the line position measurements is dependent upon the accuracy of the calibration standards. The accuracy of positions of the strong unblended ν_2 band OCS lines used for wavenumber calibration is of the order of $1–3 \times 10^{-6}\,cm^{-1}$[12]. Because of overlap and high density of spectral lines in the CH_3CN ν_4 band, the accuracy in measured line positions is an order of magnitude worse compared with the accuracy of the standards used. The positions of the majority of strong, unblended lines (see Supplementary List) are measured to an accuracy of $1–3 \times 10^{-5}\,cm^{-1}$. Positions of most of the other measured lines are accurate to a few times $10^{-4}\,cm^{-1}$. The line intensities and pressure-broadened half-width coefficients for strong, unblended lines are determined to a few tenths of 1%. Considering the (unknown) systematic uncertainties in sample pressures and temperatures, absorption path length, and volume-mixing ratio determinations of CH_3CN in the N_2-broadened data, the absolute accuracies in intensities and half-width coefficients are limited to 1% and 2%, respectively. In many cases, especially for N_2 broadening, the measured pressure-induced shift coefficients provide only upper limits since their uncertainties are comparable to the measured values.

3.5. Comparison with prior broadening studies

Except for [36], previous measurements of self- and N_2-broadening for CH_3CN have been reported mainly for microwave and far-infrared transitions of the main isotopolog [36–45] and often involved just a handful of transitions at low J. In 1989, Buffa et al. [38] reported that widths and shifts calculated with semi-classical

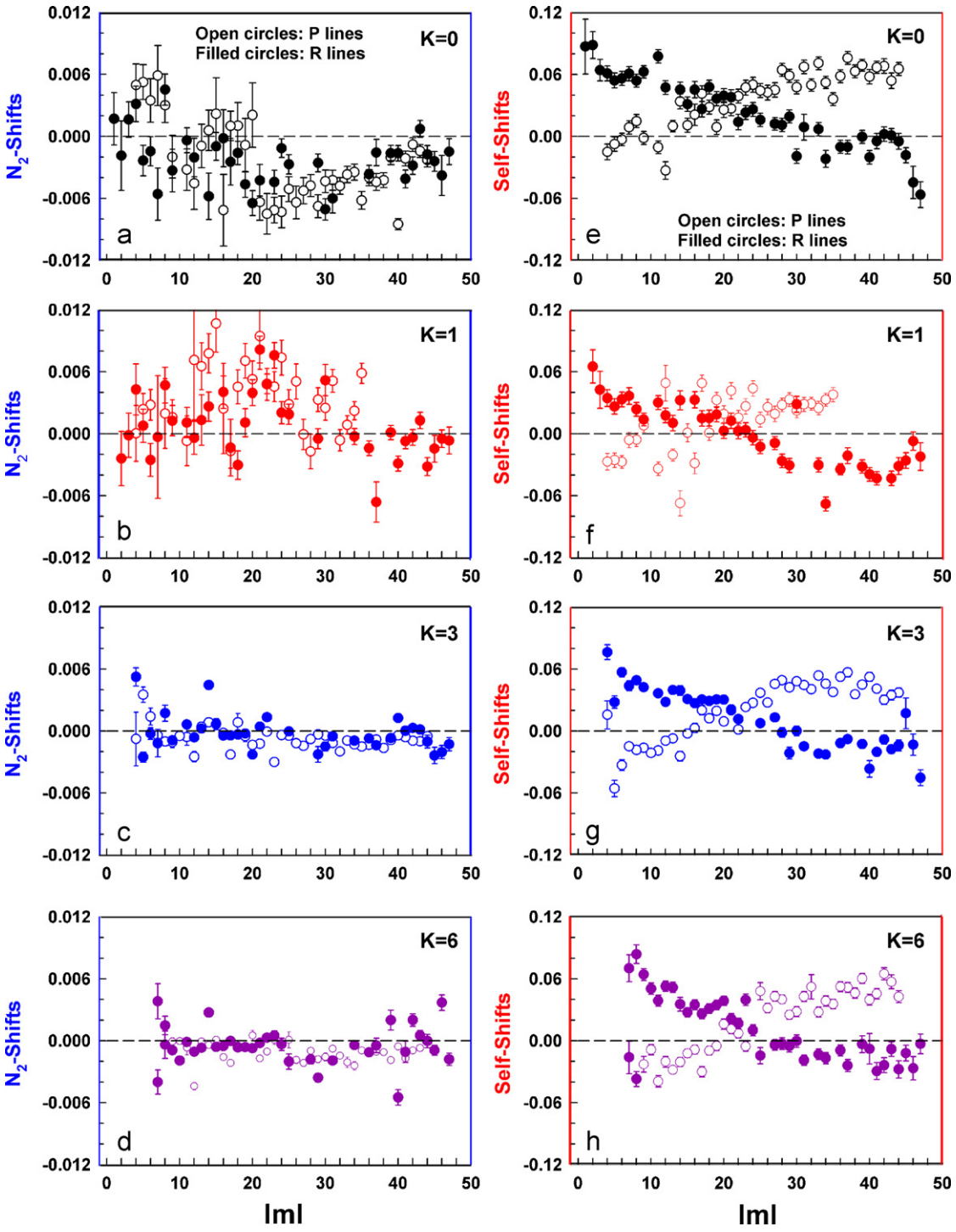

Fig. 9. N_2-shift (left side panels) and self-shift (right side panels) coefficients in $cm^{-1}\,atm^{-1}$ at ~294 K plotted as a function of $|m|$ for several select values of K. The horizontal dashed line represents a pressure-induced shift coefficient of zero. Where no error bars are visible, the uncertainties in the measurements are smaller than the size of the symbols used. See text for details.

models [46] were higher than available observed low J measurements. In 1992, Buffa et al. [42] measured self-broadening at low J and presented a prediction that resembled the patterns observed in the present ν_4 data (see Fig. 4 of that paper); they also noted that their results and those of Fabian et al. [43] were lower than the

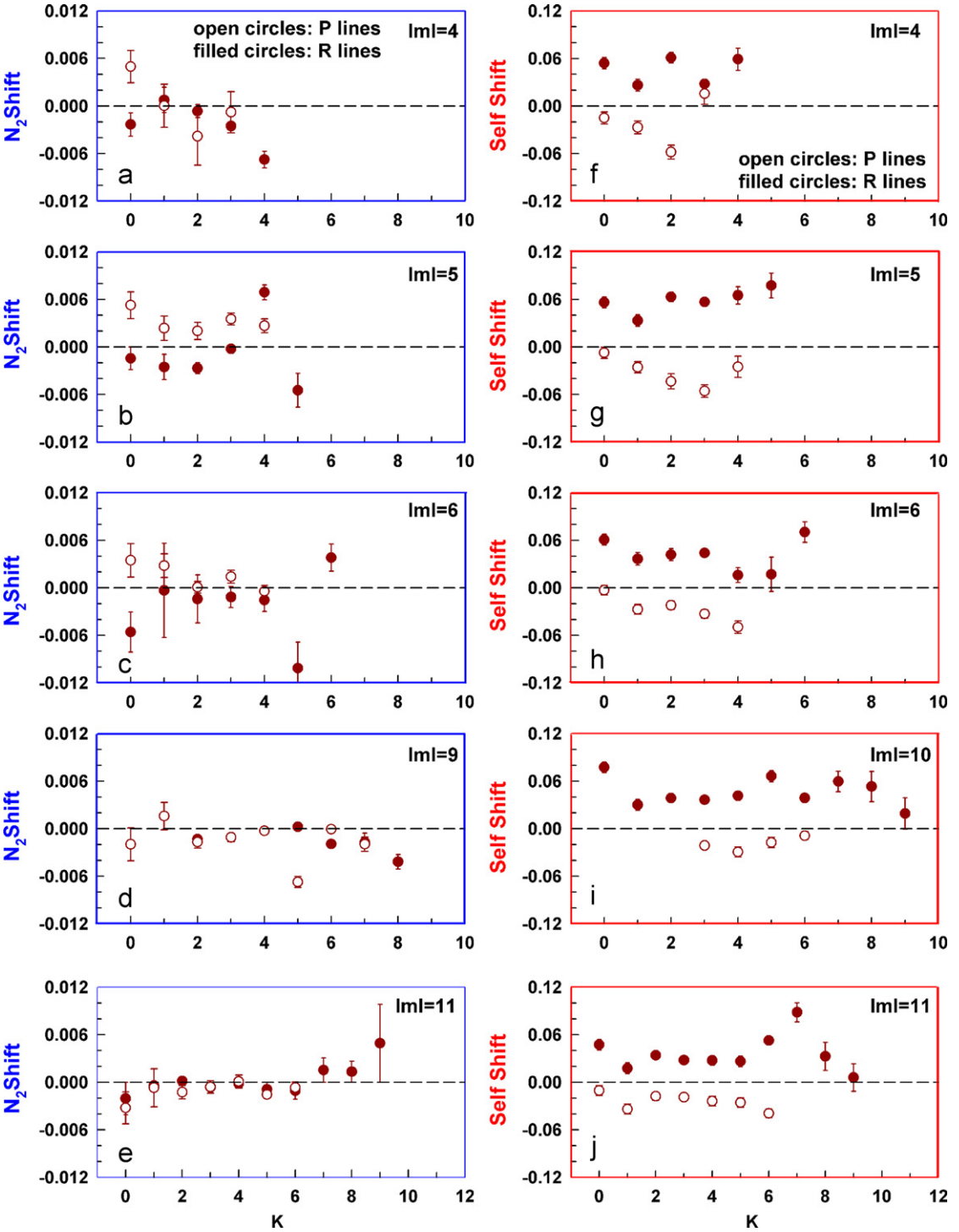

Fig. 10. N_2-shift (left panels) and self-shift (right panels) coefficients in $cm^{-1}\,atm^{-1}$ at ~294 K plotted as a function of K for lines in select series of $|m|$. The horizontal dashed line represents a pressure-induced shift coefficient of zero. Where no error bars are visible, the uncertainties in the measurements are smaller than the size of the symbols used. See text for details.

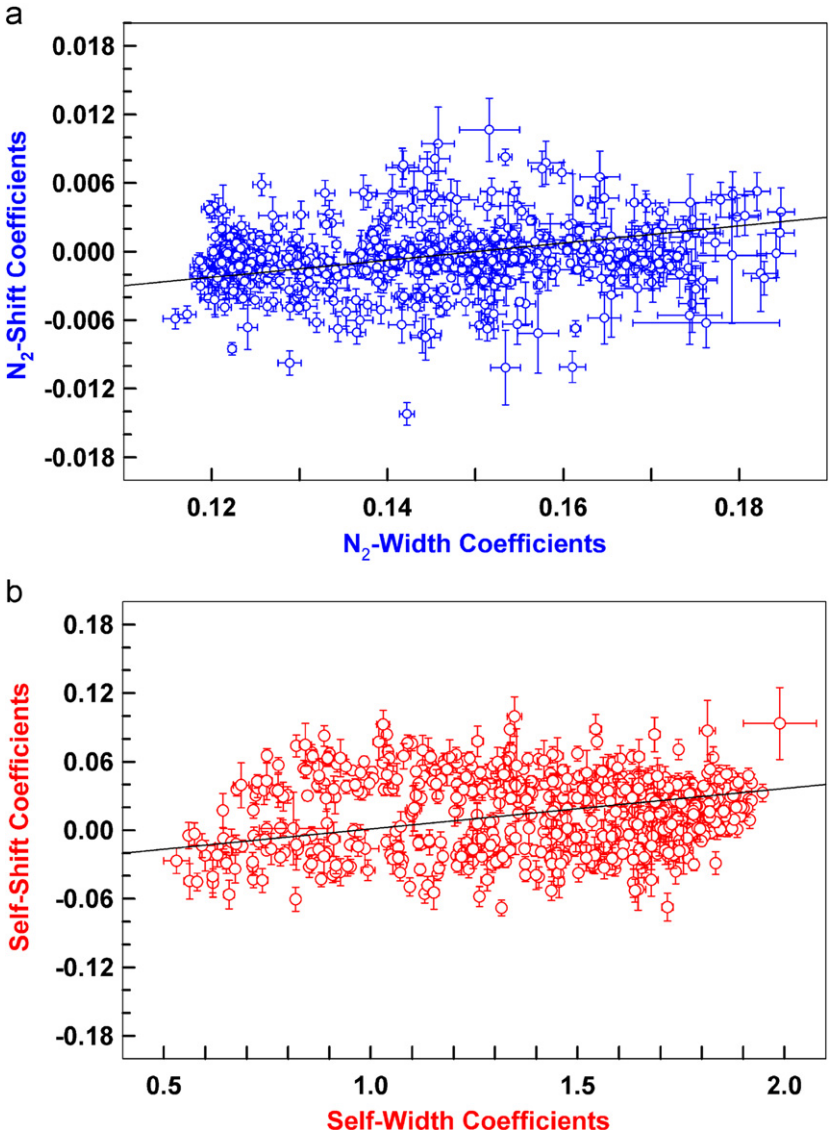

Fig. 11. (a) N_2-shift coefficients in $cm^{-1}\,atm^{-1}$ at ~294 K are plotted vs. N_2-broadened half-width coefficients in $cm^{-1}\,atm^{-1}$ at 296 K. (b) Self-shift coefficients in $cm^{-1}\,atm^{-1}$ at ~294 K are plotted vs. self-broadened half-width coefficients in $cm^{-1}\,atm^{-1}$ at 296 K. In both cases, a small positive correlation between the shift and width coefficients is evident. Where no error bars are visible, the uncertainties in the measurements are smaller than the size of the symbols used.

predicted values. Schwaab et al. [44] later measured self-broadened widths and shifts for the R42, R43, R55, and R67 manifolds and demonstrated that the calculated values were even higher than observed (by 35–50%). The most recent study by Colmont et al. [45] included broadening measurements by foreign gas (N_2) for a dozen rotational transitions in the R11 manifold for $K = 0 \rightarrow 11$. These authors also reported a value of the temperature-dependence coefficient for one transition for N_2-widths of 0.71, which is similar to those of Derozier et al. [41] and very close to the value of 0.75 assumed in this study. As seen in Table 6, the present and Colmont et al. [45]-observed N_2-broadened half-width coefficients are in excellent agreement, although present values are slightly higher. In Table 6, a comparison of the predicted values presented by Colmont et al. [45] using the formulation of Robert and Bonamy [47] is made. The mean difference %(calc−obs)/obs for 10 lines is $1.3 \pm 2.7\%$, suggesting that the current models can predict the N_2-broadened widths for the ν_4 band of CH_3CN with accuracies sufficient for studies involving Titan.

Table 6
Comparison of N_2-broadened CH_3CN widths[a]

J'	K'	J''	K''	g_s–g_s widths	v_4 widths	% dif obs–obs	% dif g_s calc−v_4
12	0	11	0	0.164	0.166	−1.2	3.7
12	1	11	1	0.164	0.168	−2.4	1.8
12	2	11	2	0.163	0.164	−0.6	3.7
12	3	11	3	0.160	0.163	−1.9	3.4
12	4	11	4	0.158	0.162	−2.5	2.4
12	5	11	5	0.159	0.159	−0.0	2.7
12	6	11	6	0.153	0.157	−2.6	0.7
12	7	11	7	0.146	0.154	−4.8	−1.0
12	8	11	8	0.144	0.148	−2.1	−1.7
12	9	11	9	0.134	0.145	−7.4	−4.7

Note: (g_s–g_s) are half-width coefficients of rotational transitions at 303 K taken from Table 3 of Colmont et al. [45] and corrected to corresponding half-width coefficients at 296 K using $n = 0.71$. Their calculation of g_s–g_s half-width coefficients (g_s calc) utilized the Robert–Bonamy formulation [47]. The v_4 values are from the present study.

[a]The half-width coefficients (widths) are in $cm^{-1}\,atm^{-1}$ at 296 K.

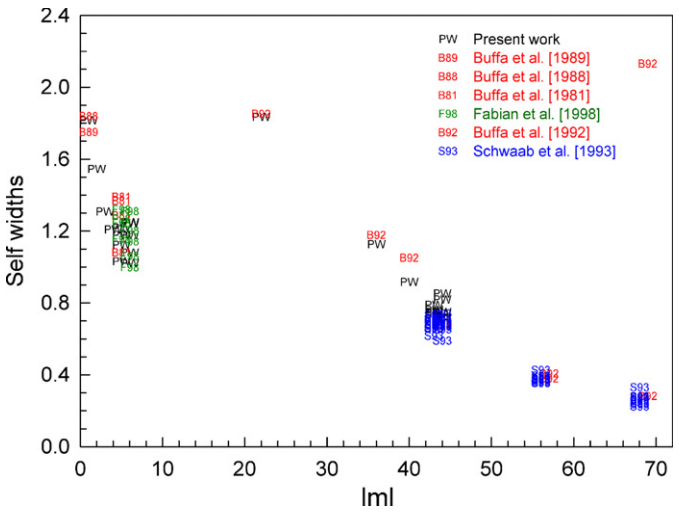

Fig. 12. Comparison of self-width coefficients reported previously in the rotational [38,41,43], millimeter [39] and far-infrared transitions [42,44] with present measurements.

In contrast, some pressure-induced line shift coefficients were previously reported for a few rotational transitions (see [37,38,40,41,43] and the references therein) but with accuracies worse than those obtained for strong, well-separated transitions in the present study of v_4; subsequently, the agreement with the present study is poor.

In Fig. 12, we compare the self-broadened half-width coefficients reported in the rotational and far-infrared regions discussed above with present measurements. Good agreement is seen in most cases; the ratios of 39 self-broadened half-width coefficients from the prior studies to present values give a mean and standard deviation of 1.00 ± 0.10. Because of the smaller number (17) of self-shift coefficients that are available compared with the self-broadened half-width coefficients, and also due to the larger relative uncertainties associated with the shift coefficients, the mean and standard deviations in the ratios of self-shift coefficients from prior studies to present measurements are found to be 1.3 ± 1.4.

4. Summary and conclusions

Room-temperature values of line positions, intensities, nitrogen (N_2)- and self-broadened half-width coefficients and pressure-induced line shift coefficients have been derived for over 700 individual transitions

from the analysis of 0.0016 cm^{-1} resolution laboratory absorption spectra of the parallel v_4 band of CH_3CN located near 920 cm^{-1}. Although the ratio of self- to N_2-broadened widths shows compact, well-defined, and similar distributions in the P and R branches, the distributions are different as a function of K. Shifts vs. $|m|$ for $|m| < \sim 45$ have been derived for both self- and N_2-broadening. Self-shift coefficients are large and both negative and positive. A calculation of the total internal partition function has also been performed, and the results have been made available to databases for atmospheric and planetary science investigations [15,16]. The present results have been obtained from spectra recorded near room temperature and are directly applicable to measurements of the Earth's atmosphere. Additional measurements of widths and shifts at lower temperatures are needed, for example, to aid in interpreting the stratospheric measurements of Titan's atmosphere obtained by the CIRS Fourier transform spectrometer [6,7] and for measurements of comets [4] and the interstellar medium. A global analysis of line positions and intensities is in progress.

A list of spectral line parameters including positions, intensities, and assignments for the pure rotational and rovibrational transitions will eventually become available in the Cologne Database for Molecular Spectroscopy (CDMS) [48,49].

Acknowledgments

The experimental work for this paper was performed at the W.R. Wiley Environmental Molecular Sciences Laboratory, a national scientific user facility sponsored by the Department of Energy's Office of Biological and Environmental Research and located at Pacific Northwest National Laboratory. PNNL is operated for the United States Department of Energy by the Battelle Memorial Institute under Contract DE-AC05-76RLO 1830. NASA's planetary atmospheres program supported the work performed at NASA Langley Research Center and the College of William and Mary. Research at the Jet Propulsion Laboratory (JPL), California Institute of Technology, was performed under contract with the National Aeronautics and Space Administration. H.S.P.M. and the CDMS are supported by the Bundesminiterium für Bildung und Forschung (BMBF) administered through Deutsches Zentrum für Luft- und Raumfahrt (DLR; the German space agency). Two of us (R.R.G. and D.L.N.) are pleased to acknowledge support of this research by the National Science Foundation through Grant no. ATM-0242537. Any opinions, findings, and conclusions or recommendations expressed in this material are those of the author(s) and do not necessarily reflect the views of the National Science Foundation. I.K. and A.D.-K. wish to thank the Programme National de Planétologie (PNP, France) for their funding of the project.

Appendix A. Supplementary materials

Supplementary data associated with this article can be found in the online version at doi:10.1016/j.jqsrt.2007.11.013

References

[1] Livesey NJ, Fromm MD, Waters JW, Manney GL, Santee ML, Read WG. Enhancements in lower stratospheric CH_3CN observed by the upper atmosphere research satellite microwave limb sounder following boreal forest fires. J Geophys Res 2004;109 [paper no. 10.1029.2003JD004055].

[2] Livesey NJ, Waters JW, Rhosvari R, Brasseur GB, Tyndall TS, Read W. Stratospheric CH_3CN from the UARS microwave limb sounder. Geophys Res Lett 2001;28:779–82.

[3] Kleinböhl A, Toon GC, Sen B, Blavior J-F, Weisenstein D, Wennberg PO. Infrared measurements of atmospheric CH_3CN. Geophys Res Lett 2005 [paper no. 10.1029GL024283].

[4] Biver N, Bockelée-Morvan D, Crovisier J, Lis DC, Moreno R, Colom P, et al. Radio wavelength molecular observations of comets C/1999 T1 (McNaught-Hartley), C/2001 A2 (LINEAR), C/2000 WM_1 (LINEAR) and 153P/Ikeya-Zhang. Astron Astrophys 2006;449:1255–70.

[5] Watson C, Churchwell E, Pankonin V, Bieging JH. Arcsecond images of CH_3CN toward W75N. Astrophys J 2002;577:260–4.

[6] Lorentz R, Mitton J. Lifting Titan's veil: exploring the giant moon of Saturn. Cambridge: Cambridge University Press; 2002. 260p.

[7] Coustenis A, Achterberg RK, Conrath BJ, Jennings DE, Marten A, Gautier D, et al. The composition of Titan's stratosphere from Cassini/CIRS mid-infrared spectra. Icarus 2007;189:35–62.

[8] Bézard B, Martin A, Paubert G. Detection of acetonitrile on Titan. Bull Am Astron Soc 1993;25:1100.

[9] Marten A, Hidayat T, Biraud Y, Moreno R. New millimeter heterodyne observations of Titan: vertical distributions of nitriles HCN, HC_3N, CH_3CN, and the isotopic ratio $^{15}N/^{14}N$ in its atmosphere. Icarus 2002;158:532–44.
[10] Benner DC, Rinsland CP, Malathy Devi V, Smith MAH, Atkins DA. A multispectrum nonlinear least squares fitting technique. JQSRT 1995;53:705–21.
[11] Rinsland CP, Sharpe SW, Sams RL. Temperature-dependent infrared absorption cross-sections of methyl cyanide (acetonitrile). JQSRT 2005;96:271–80.
[12] Maki AG, Wells JS. Wavenumber calibration tables for heterodyne frequency measurements. Diane Publishing; 1991 [also available as NIST (National Institute of Standards and Technology) special publication 821 at ⟨www. phys.nist.gov⟩].
[13] Benner DC, Malathy Devi V, Miller CE, Brown LR. Manuscript in preparation.
[14] Letchworth KL, Benner DC. Rapid and accurate calculation of the Voigt function. JQSRT 2007;107:173–92.
[15] Rothman LS, Jacquemart D, Barbe A, Benner DC, Birk M, Brown LR, et al. The HITRAN 2004 molecular spectroscopy database. JQSRT 2005;96:139–204.
[16] Jacquinet-Husson N, Scott NA, Chédin A, Garceran K, Armante R, Chursin AA, et al. The 2003 edition of the GEISA/IASI spectroscopic database. JQSRT 2005;95:429–67.
[17] Verdes CL, Englen A, Buehler SA, Perrin A. Partition function data and impact on retrieval quality for an mm/sub-mm limb sounder. JQSRT 2005;90:217–38.
[18] Herzberg G. Introduction molecular spectra and molecular structure II. Infrared and Raman spectra of polyatomic molecules. New York: Van Nostrand Co.; 1960.
[19] Duncan JL, McKean DC, Tullini F, Nivellini GD, Perez Peńa J. Methyl cyanide: spectroscopic studies of isotopically substituted species and the harmonic potential function. J Mol Spectrosc 1978;69:123–40.
[20] Paso R, Anttila R, Koivusaari M. The infrared spectrum of methyl cyanide between 1240 and 1650 cm^{-1}: the coupled band system v_3, v_6^{+1}, and $v_7+v_8^{+2}$. J Mol Spectrosc 1994;165:470–80.
[21] Tolonen A-M, Koivusaari M, Paso R, Schroderus J, Alanko S, Anttila R. The infrared spectrum of methyl cyanide between 850 and 1150 cm^{-1}: analysis of the v_4, v_7, and $2v_8^1$ bands with resonances. J Mol Spectrosc 1993;104:383–401.
[22] Koivusaari M, Tolonen A-M, Paso R, Schroderus J, Anttila R. The $2v_8$ band of CH_3CN. J Mol Spectrosc 1993;160:566–73.
[23] McDowell RS. Rotational partition functions for symmetric-top molecules. J Chem Phys 1990;93:2801–11.
[24] Šimeckova M, Urban S, Fuchs U, Lewen F, Winnewisser G, Morino I, et al. Ground state spectrum of methylcyanide. J Mol Spectrosc 2004;226:123–36.
[25] Boucher D, Burie J, Bauer A, Dubruille A, Demaison J. Microwave spectra of molecules of astrophysical interest. XIX. Methyl cyanide. J Phys Chem Ref Data 1980;9:659–720.
[26] Pickett HM, Poynter RL, Cohen EA, Delitsky ML, Pearson JC, Müller HSP. Submillimeter, millimeter and microwave spectral line catalog, 1996 ed. JPL Publication 80-23, Rev. 4. Pasadena, CA: Caltech, 1996.
[27] Norton RH, Rinsland CP. ATMOS data processing and science analysis methods. Appl Opt 1991;30:389–400.
[28] Cazzoli G, Puzzarini C. The lamb-dip spectrum of methyl cyanide: precise rotational frequencies and improved ground-state rotational constants. J Mol Spectrosc 2006;240:153–63.
[29] Pavone FS, Zink LR, Prevedelli M, Inguscio M, Fusina P. Tunable FIR spectroscopy of CH_3CN between 569 GHz and 1.47 THz. J Mol Spectrosc 1990;144:45–50.
[30] Antilla R, Hornemann VM, Koivusaari M, Paso R. Ground-state constants A_0 D_0^K of CH_3CN. J Mol Spectrosc 1993;157:198–207.
[31] Müller HSP, Drouin BJ, Pearson JC, Brown LR, Kleiner I, Dahayem A, et al. Rotational spectroscopy as a tool to investigate interactions between vibrational polyads in symmetric top molecules: low lying states of methyl cyanide. In: Proceedings of the 62nd symposium on molecular spectroscopy, Columbus, OH, USA, Paper WG03, 2007.
[32] Bocquet R, Wlodarczak G, Bauer A, Demaison J. The submillimeter-wave rotational spectrum of methyl cyanide: analysis of the ground and low-lying vibrational states. J Mol Spectrosc 1988;127:382–9.
[33] Koivusaari M, Horneman K-M, Antilla R. Infrared bands v_8 and $2v_8$ of CD_3CN. J Mol Spectrosc 1991;149:227–57.
[34] Tarrago G. The pentad $2v_2$, v_2+v_4, $2v_4$, v_1, and v_3 of PH_3: theoretical background and analysis programs. J Mol Spectrosc 1990;139:439–45.
[35] Malathy Devi V, Benner DC, Smith MAH, Rinsland CP, Predoi-Cross A, Sharpe SW, et al. A multispectrum analysis of v_2 band of $H^{12}C^{14}N$: Part I. Intensities, broadening, and shift coefficients. JQSRT 2005;231:66–84.
[36] Hajsaleh J, Al-Share M, Johri M, Johri GK, Roberts JA. An experimental study of collision broadening of rotational spectral lines of $^{13}CH_3^{13}C^{15}N$ in the ground and nv_8, $n=1$ and 2 vibrationally excited states at microwave frequencies. J Chem Phys 1992;96:3416–21.
[37] Srivastava GP, Gautam HO, Kumar A. Microwave pressure broadening studies of some molecules. J Phys B Mol Phys 1973;6:743–56.
[38] Buffa G, Giulietti M, Lucchesi M, Matinelli M, Tarrini O. Collisional line shape for the rotational spectrum of methycyanide. J Chem Phys 1989;90:6881–6.
[39] Buffa G, Dilieto A, Minguzzi P, Tonelli M. Acoustic detection in millimeter wave spectroscopy—pressure broadening of CH_3CN. Int J Infrared Millimeter Waves 1981;2:559–69.
[40] Buffa G, Giulietti D, Lucchesi M, Martinelli M, Tarrini O, Zucconi M. High-resolution measurements of pressure self-broadening and shift for the methyl-cyanide rotational $J=1$–0 line. Nuovo Cimento Soc Ital Fis D Condens Matter Atom Mol Chem Phys Fluids Plasmas Biophys 1988;10:511–8.
[41] Derozier D, Rohart F. Foreign gas and self-relaxation of CH_3CN: low-temperature dependence for the 92-GHz transition. J Mol Spectrosc 1990;96:1–12.

[42] Buffa G, Tarrini O, De Natale P, Inguscio M, Pavone FS, Prevedelli M, et al. Far infrared self-broadening in methylcyanide: absorber–perturber resonance. Phys Rev A 1992;45:6443–50.
[43] Fabian M, Morino I, Yamada KMT. Analysis of the line profiles of CH_3CN for the $J = 5 \rightarrow 4$ and $J = 6 \rightarrow 5$ rotational transitions. J Mol Spectrosc 1998;190:232–9.
[44] Schwaab GW, Evenson KM, Zink LR. Far-infrared self-broadening and pressure shift measurements of methyl cyanide. Int J Infrared Millimeter Waves 1993;14:1643–55.
[45] Colmont JM, Rohart F, Wlodarczak, Boyanich JP. *K*-dependence and temperature dependence of N_2-, H_2- and He-broadening coefficients for the $J = 12$–11 transition of acetonitrile $CH_3C^{14}N$ located near 2007 GHz. J Mol Spectrosc 2006;238:87–107.
[46] Tsao CJ, Curnutte B. Line-widths of pressure-broadened spectral lines. JQSRT 1962;2:41–62.
[47] Robert D, Bonamy J. Short-range effects in semi-classical molecular line broadening calculations. J Phys 1979;20:923–43.
[48] Müller HSP, Thorwirth S, Roth DA, Winnewisser G. The cologne database for molecular spectroscopy. Astron Astrophys 2001;370:L49–52.
[49] Müller HSP, Schlöder F, Stutzki J, Winnewisser G. The cologne database for molecular spectroscopy, CDMS: a useful tool for astronomers and spectroscopists. J Mol Struct 2005;742:215–27.